# Interaction dynamics of two colloids in a single optical potential

Benjamin Tränkle,[1] Michael Speidel,[2] and Alexander Rohrbach[1,*]
[1]*Laboratory for Bio- and Nano-Photonics, Georges-Koehler-Allee 102, 79110 Freiburg, Germany*
[2]*Sick Stegmann GmbH, 78166 Donaueschingen, Germany*
(Received 26 January 2012; published 1 August 2012)

The interaction of two diffusing particles is strongly influenced by their hydrodynamic coupling. At a tracking rate of 10 kHz we are able to measure the 3D trajectories of two colloidal spheres in a single harmonic potential, which was generated by scanning line optical tweezers. This common potential enables tilting, rotational, and translational dynamics of the spheres, which we analyzed via the spheres position cross-correlations $C(\tau)$ over a time range of $10^{-4}$–2 s. We found that the dynamic interaction of the colloids is controlled by short-range surface forces $\boldsymbol{F}_s$, which are attractive in one direction and repulsive in the other two directions. This unexpected behavior is supported by a theoretical model using two Langevin equations, which decouple for linear $\boldsymbol{F}_s$, allowing a description with autocorrelation functions for collective and relative motions. We further demonstrate that variations in salt concentration and reaction volumes significantly influence $C(\tau)$ and the mean contact times between the particles, which may offer new insights into biological particle interaction.

DOI: 10.1103/PhysRevE.86.021401 PACS number(s): 83.80.Hj, 83.10.Pp, 83.85.Jn, 87.80.Cc

## I. INTRODUCTION

Long-range physical interactions control many short-ranged specific reactions between diffusing particles in biology, chemistry or soft matter physics [1]. Direct interactions such as electrostatic or van der Waals potentials can have interaction ranges in the order of a particle diameter [2,3]. Indirect interactions such as hydrodynamic coupling between two particles, however, can reach interaction lengths of even several particle diameters [4] and often control time-variant effects such as reactions kinetics or synchronization in biological processes [5].

A well-established method to study hydrodynamic interactions is to use colloidal spheres in confined areas or external potentials, which enhance the interaction rate significantly. Here, optical traps have become a key technology to induce colloidal interactions, since trapping potentials and volumes are easily adjustable and simultaneously tracking of the colloids translational [6] or rotational [7] motion is possible. More than a decade ago, it could be shown that the cross-correlations $C[\mathbf{r}_1(t),\mathbf{r}_2(t)] = C(\tau)$ of the position traces $\mathbf{r}_1(t)$ and $\mathbf{r}_2(t)$ of two micron-sized spheres in two adjacent point traps reveal a time-delayed anticorrelation of the sphere positions [8,9]. In contrast to free particles in an unbound fluid, where particles drag one another in the direction of motion, the cross-correlation $C(\tau)$ for two particles in an external potential is negative since their correlated motion vanishes faster than anticorrelated motion. Similar experiments for other diffusion geometries and constraints were based on this technique and analysis [6,10,11]. However, in all these studies the particles separated by the two optical potentials did never contact each other and the interaction times were limited by the relative short autocorrelation times ($\tau < 50$ ms) of optical point traps.

In this study we investigate the interaction dynamics of two spheres in a single potential, which is generated by a line optical trap enabling particles to touch each other. Thereby both long- and short-range interactions can be investigated in a time window of $\tau = 100$ $\mu$s to $\tau = 1$ s using a novel 3D tracking technique [12]. Correlations of the spheres' positions are determined both experimentally and theoretically in all three directions for various trapping volumes and electrostatic surface potentials, as well as the mean contact times between the spheres. We will show that this contact time represents a time-differential association constant and is directly connected to the relaxation time for relative motions.

## II. EXPERIMENTAL PRINCIPLE

The experimental principle is sketched in Fig. 1. A highly focused laser beam ($\lambda = 1064$ $\mu$m) is scanned with $f_{\text{scan}} =$ 10 kHz along a 10-$\mu$m-long line using an acousto-optic deflector (AOD). By modulating the transmission of the AOD, an intensity distribution with Gaussian profile of variable width can be adjusted such that a particle diffuses in an approximately 3D harmonic optical potential $V(r) = 1/2(\kappa_x x^2 + \kappa_y y^2 + \kappa_z z^2)$ with trap stiffnesses $\kappa_x < \kappa_z < \kappa_y$. This choice of trap stiffnesses permits a rather free diffusion of the particles in the $x$ direction (longitudinal motion), whereas motions in the $y$ and $z$ directions (lateral motions) are confined to a greater extent. When the laser focus sweeps over one sphere (0.97 $\mu$m, silica, Bangs labs, size variation 10–15%), light is coherently scattered and interferes with unscattered light in the back-focal plane (BFP) of a detection lens (DL). While the particles experience a time-averaged optical potential, interference peaks from the sweeping laser focus are well separable for each sphere with a single quadrant photodiode (QPD) located in a plane conjugate of the DL's BFP [12]. In our case, a second QPD increases both tracking range and linearity [13] such that the linear relation $\boldsymbol{S}_n(t) - \boldsymbol{S}_0 \approx \overleftrightarrow{g}\boldsymbol{r}_n(t)$ between signal triplet $\boldsymbol{S}_n = (S_{xn}, S_{yn}, S_{zn})$ and position triplet $\boldsymbol{r}_n = (x_n, y_n, z_n)$ is well justified ($n = 1,2$ is the particle number, $\overleftrightarrow{g}$ is the diagonal sensitivity matrix). As displayed in Fig. 1(b), the position trajectories $\boldsymbol{r}_1(t)$ and $\boldsymbol{r}_2(t)$ from both spheres diffusing in the elongated potential 30 $\mu$m away from the coverslip are tracked with $\delta t = 100$ $\mu$s resolution and 5- to

*rohrbach@imtek.de

 

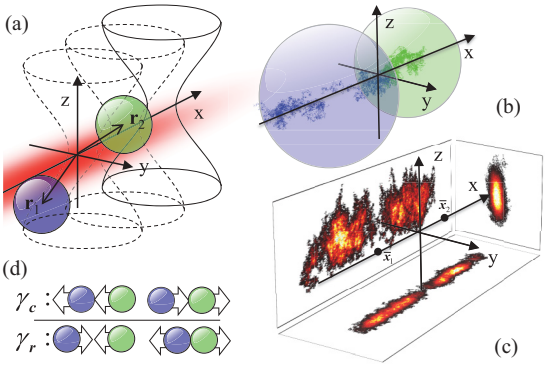


FIG. 1. (Color online) Experimental principle. (a) A laser trap is scanned in the $x$ direction at 10 kHz, generating an elongated optical potential. (b) The trajectories $r_1(t)$ and $r_2(t)$ can be recovered using back-focal plane interferometry with a quadrant photodiode. (c) Projections of the 3D position histograms of two diffusing beads in a single potential. (d) Particle diffusion can be divided into collective (drag $\gamma_c$) and relative motion (drag $\gamma_r$).

20-nm precision (see also the movies in Ref. [14]). Figure 1(c) shows the corresponding histograms of 50 000 position pairs and illustrates the different widths $\sigma_i = (k_BT/\kappa_i)^{1/2}$ of the harmonic potentials in directions $i = (x,y,z)$. Here $k_BT \approx 4 \times 10^{-21}$ J is the thermal energy.

## III. STATIC AND DYNAMIC INTERACTIONS

### A. Hydrodynamic interactions

Neglecting rotation, the translational diffusion of two spheres in a common harmonic potential with diagonal stiffness matrix $\overleftrightarrow{\kappa}$ can be expressed by two coupled Langevin equations

$$\begin{pmatrix} \boldsymbol{v}_1 \\ \boldsymbol{v}_2 \end{pmatrix} = \begin{pmatrix} \mu_{11}(\boldsymbol{R}) & \mu_{12}(\boldsymbol{R}) \\ \mu_{12}(\boldsymbol{R}) & \mu_{11}(\boldsymbol{R}) \end{pmatrix} \begin{pmatrix} \boldsymbol{F}_{\mathrm{th}1} + \boldsymbol{F}_{s1} - \overleftrightarrow{\kappa}\, \boldsymbol{r}_1 \\ \boldsymbol{F}_{\mathrm{th}2} + \boldsymbol{F}_{s2} - \overleftrightarrow{\kappa}\, \boldsymbol{r}_2 \end{pmatrix}, \quad (1)$$

where the function $\boldsymbol{F}_{\mathrm{th}}(t)$ accounts for the stochastic forces satisfying $\langle \boldsymbol{F}_{\mathrm{th}} \rangle = 0$ and $\langle \boldsymbol{F}_{\mathrm{th}n}(t), \boldsymbol{F}_{\mathrm{th}m}(t') \rangle = 2k_BT\mu_{nm}^{-1}\delta(t - t')$. $\mu_{nm}(\boldsymbol{R})$ is the mobility matrix, which couples the particles' velocities $\boldsymbol{v}_n$ and $\boldsymbol{v}_m$ as a function of the center-to-center distance $R = |\boldsymbol{R}| = |\boldsymbol{r}_1 - \boldsymbol{r}_2|$. In addition, particle coupling is mediated by a distance-dependent surface force $\boldsymbol{F}_{sn}(\boldsymbol{R})$. In the case of two point traps and vanishing interaction forces $\boldsymbol{F}_{sn}(\boldsymbol{R})$, the beads have a constant mean distance and the Langevin equations of spheres 1 and 2 can be decoupled by using a new set of collective (index $c$) and relative (index $r$) coordinates, $x_{ic} = (x_{i1} + x_{i2})/\sqrt{2}$ and $x_{ir} = (x_{i1} - x_{i2})/\sqrt{2}$. As illustrated in Fig. 1(d), the resulting collective and relative motions of two spheres have different viscous drags, $\gamma_c < \gamma_r$. The mobility coefficients $\mu_{ij}(R)$ for motions described by these coordinates are well-known functions of the particles' distance $R$ and can be expressed by an expansion series in terms of $1/R$ [15].

The cross-correlation functions of two spheres $C_i(x_{i1},x_{i2})$ can be expressed by a superposition of the autocorrelation functions $A_i(\tau)$ of the eigenmodes, $C_i(x_{i1},x_{i2}) = 1/2[A_i(x_{ic}) - A_i(x_{ir})]$ [8,16] such that $C_i(\tau) = k_BT/2\kappa_i[\exp(-\tau\mu_c\kappa_i) - \exp(-\tau\mu_r\kappa_i)]$ is negative.

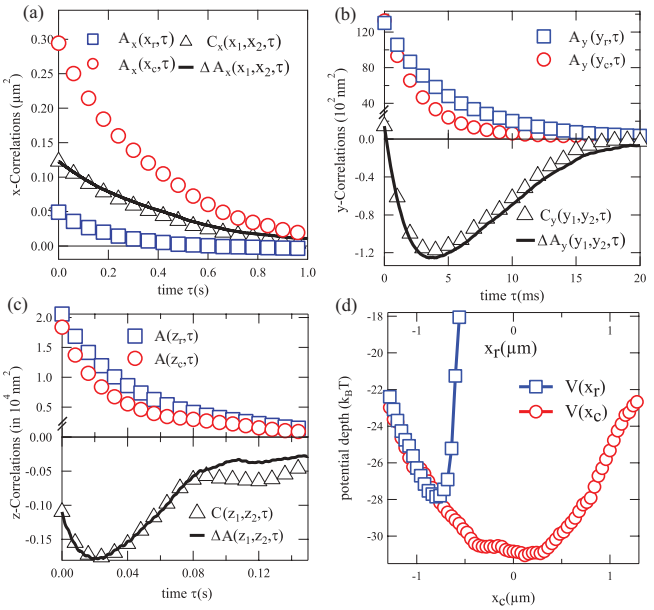


FIG. 2. (Color online) Cross-correlations and difference of autocorrelations. [(a)–(c)] Autocorrelation functions for $x$, $y$, and $z$ fluctuations of the correlated (◯) an relative (□) coordinates. The cross-correlation functions $C(x_{i1},x_{i2},\tau)$ are depicted with black triangles. The difference function $\Delta A_i = 1/2(A_{ic} - A_{ir})$ is indicated by the black line. (d) Potentials corresponding to collective (◯) and relative motions (□) in the $x$ direction.

Due to hydrodynamic coupling, the decay times $\tau_c = \gamma_c/\kappa$ and $\tau_r = \gamma_r/\kappa$ for these modes differ, i.e., the mobility of relative motions is decreased, whereas the collective mobility is increased ($\mu_c > \mu_r$ or $\tau_c < \tau_r$). Therefore, the cross-correlation functions also show a distinct dependency on the mean particle separation $\overline{R}$, i.e., hydrodynamic coupling gets more pronounced for decreasing $\overline{R}$.

### B. Static interactions

The situation changes when the two spheres can touch each other and short-range interactions must be taken into account. In general, the interparticle force $F_s(R)$ is a nonlinear function of the distance $R$ of the two spheres. Whereas the hydrodynamic coupling affects both the collective and relative modes of motion, a static coupling $C(\tau = 0)$ as from pair potentials affects only relative particle motions. Even though transmitted by the fluid, lubrication forces solely take effect in relative motion and increase with decreasing $R$ [17,18]. Furthermore, in a single potential, all particle distances $R$ occur and thereby $\mu_{nm}(R)$ varies.

### C. Superposition of correlation functions

The question is whether the cross-correlation $C(\tau)$ in the direct contact situation can be still expressed by the autocorrelations of the collective and relative motions. Figure 2 displays, by use of the black curves (△), a typical set of cross-correlations $C_i(x_{i1},x_{i2})$ obtained from experimental data in the $x$ direction (a), $y$ direction (b), and $z$ direction (c). Furthermore, the same data were used to calculate collective and relative trajectories $\boldsymbol{r}_c(t)$ and $\boldsymbol{r}_r(t)$ and the autocorrelation

function of these coordinates. The autocorrelation functions $A_i(x_{ic})$ and $A_i(x_{ir})$ are shown in Figs. 2(a)–2(c) with the red (◯) and blue (□) lines, respectively. We also computed the differences $\Delta A_i(\tau)$ of the two autocorrelation functions, $\Delta A_i(\tau) = 1/2[A_i(x_{ic},\tau) - A_i(x_{ir},\tau)]$, which are plotted as black lines in Figs. 2(a)–2(c). As the first result of this study, we find a good coincidence between $C_i(\tau)$ and $\Delta A_i(\tau)$ in all three dimensions, demonstrating that the cross-correlation $C_i(\tau)$ of two particles in a single potential still can be understood as a superposition of the autocorrelation functions of correlated and anticorrelated motion. It is noted that for nearly touching spheres, we find a systematic tracking error. However, this position error hardly affects the shape of the resulting $C_i(\tau)$ (see S1 in Ref. [14]).

## IV. CROSS-CORRELATION FUNCTIONS OF TWO SPHERES IN A SINGLE POTENTIAL

Based on the analysis principles for two point traps, we approximate the elongated common potential to be a superposition of many point traps with mean separations $\overline{R} \in [R_{\min}, R_{\max}]$. We therefore average over all correlation functions $C_i(x_{i1},x_{i2},\overline{R})$ such that

$$C_i(x_{i1},x_{i2}) = \int_{R_{\min}}^{R_{\max}} \frac{1}{2} p(\overline{R})\big[A_i(x_{ic}) - A_i(x_{ir})\big] d\overline{R}. \quad (2)$$

Here, $p(\overline{R})$ denotes the equilibrium probability to find the two beads at mean separation according to the local potential depth $V(R)$. Figure 2(d) depicts the Boltzmann potentials for the collective modes in the $x$ direction $V(x_c) = -k_BT\ln[p(x_c)] + V_{0c}$ and the asymmetric interaction potential $V(x_r) = -k_BT\ln[p(x_r)] + V_{0r}$ for relative motion.

A further crucial question is whether and how information about the short-range interaction between both spheres can be extracted from the position cross-correlations. To derive an expression for the distance-variant coupling, we approximate the surface force in direction $i$ to be linear, $F_{is} \approx \kappa_{is}(x_{i1} - x_{i2})$, and the changes in mobility to be small such that $\mu_{ic}(R) \approx$ const and $\mu_{ir}(R) \approx$ const. It is straightforward to see that the additional force in Eq. (1) cancels out for the correlated motions, since $F_{is1} = -F_{is2}$. Thereby the Langevin equations are linearized and can be decoupled by using normal coordinates for relative and collective motions (see also S2 in Ref. [14]). For direction $x_i$ we derive

$$C_i(\tau) = \frac{k_BT}{\kappa_i} e^{-\tau/\tau_{ic}} - \frac{k_BT}{\kappa_i + 2\kappa_{is}} e^{-\tau/\tau_{ir}}, \quad (3)$$

with autocorrelation times $\tau_{ic}(R) = \gamma_{ic}(R)/\kappa_i$ and $\tau_{ir}(R) = \gamma_{ir}(R)/(\kappa_i + 2\kappa_{is})$. Here, the decay time $\tau_{ir}$ is altered by the additional force constant $\kappa_{is}$ of the particle interaction force. The analytical expressions in Eqs. (2) and (3) now enable a qualitative explanation of the curves in Fig. 2. Both the amplitudes and the decays of the exponentials in Eq. (3) differ according to the force constants for relative and collective modes.

### A. Longitudinal motions

For the longitudinal motions mutual passage of the particles is excluded and relative diffusion in the $x$ direction takes place in a steeper potential [see Fig. 2(d)]. The increase of the effective force constant for relative modes in the $x$ direction reduces the relative fluctuation widths $\sqrt{\langle x_{ir1}^2\rangle\langle x_{ir2}^2\rangle}$ and $C_x$ becomes positive [Fig. 2(a)].

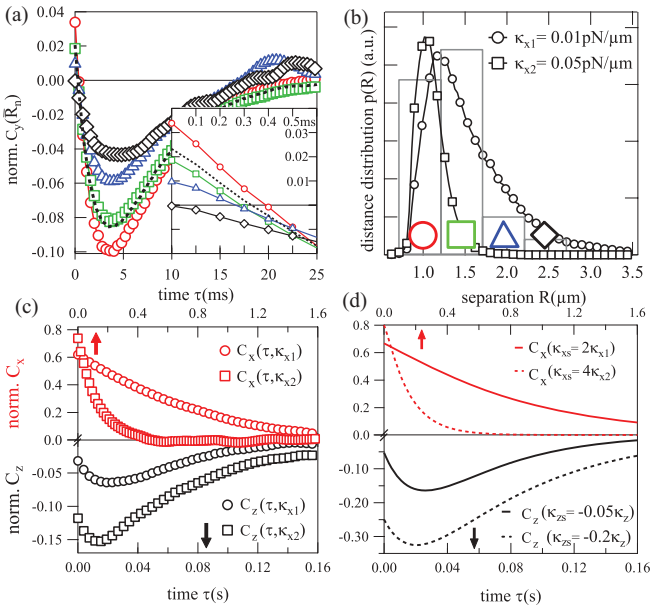


FIG. 3. (Color online) Interaction dynamics varying with the fluctuation direction. (a) Normalized cross-correlation functions $C_y$ at four distinct mean separations. The dashed line represents a superposition according to Eq. (3), and the symbols correspond to regions in (b). The inset shows the same curves for short time scales. (b) Probability distributions $p(R,\kappa)$ for two different trap stiffnesses $\kappa_x$ to find the beads at a distance $R$. (c) $C_x$ and $C_z$ for two different trap stiffnesses $\kappa_{x1}$ and $\kappa_{x2} = 5\kappa_{x1}$ in the $x$ and $z$ directions. (d) Theoretical curves according to the model of Eq. (3) with $\gamma_r = 2\gamma_c, \kappa_{xs} = 2\kappa_{x1}, \kappa_{zs} = -0.05\kappa_z$ (solid lines) and $\kappa_{xs} = 4\kappa_{x2}, \kappa_{zs} = -0.2\kappa_z$ (dashed lines).

### B. Lateral motions

In lateral direction, a repulsive surface force $\boldsymbol{F}_s$ counteracts the trapping force $\boldsymbol{F}_{\text{opt}}$ and facilitates relative diffusion. Moreover, the particles touching each other tend to evade the longitudinal force $F_{x,\text{opt}} \approx \kappa_x x$ such that $\Delta x < 2R$. In this case, the axis connecting the spheres is tilted and $C_z < 0$ (see Fig. S2(b) in Ref. [14]). This tilting occurs most likely in the $z$ direction, where $F_{z,\text{opt}} \approx \kappa_z z < \kappa_y y$. The static coupling results in a correlation function that is also negative for $\tau \to 0$. In the $y$ direction, we find the cross-correlation function to be negative on longer, but positive on short, time scales [Figs. 2(b) and 3(a)]. In the submillisecond range, collective modes dominate and tilting and electrostatic forces, which only affect relative modes, are less important. According to our model, $\kappa_{ys}$ must be negative, which would require a yet-unknown attractive surface force in the $y$ direction. It seems possible that a hydrodynamic wake or lubrication forces lead to a positive $C_y$ on short time scales, whereas on longer time scales this effect is hardly visible. The approximation of a line potential allowing many several mean distances $\overline{R}$ by several point traps according to Eq. (2) was further tested.

## V. IMPACT OF STATIC INTERACTIONS

### A. Distance dependency

Since the lateral potential in the $y$ direction is stiffer than in the longitudinal $x$ direction ($\kappa_x \ll \kappa_y$), the time for the particle to explore the potential along $x$ by diffusion takes much longer. Therefore, we were able to separate four different diffusion regions ($N = 1 \ldots 4$) with a mean particle separation $\overline{R}_N$ and to measure the cross-correlations $C_y(y_1, y_2, \overline{R}_N)$ [see Fig. 3(b)]. A set of cross-correlation functions $\langle y_1(\tau), y_2(\tau)\rangle / \sqrt{\langle y_1(\tau)^2\rangle \langle y_2(\tau)^2\rangle}$, normalized by the standard deviation, is depicted in Fig. 3(a) for $y$-fluctuation data at several distances. For larger $\overline{R}_N$, positive correlations vanish on short time scales [black symbols in Fig. 3(a)] and we find $C_y(\tau)$ to be very similar compared to results known from the double point-trap experiments at fixed separations. For smaller $\overline{R}_N$, $C_y(\tau)$ gets more pronounced in positive and negative amplitudes. Here, the increasing influence of short-range interactions described by $\kappa_{is}$ on particle dynamics becomes noticeable and leads to positive values in $C_y(\tau)$ at short times $\tau$ according to Eq. (3).

### B. Varying the interaction propability by $\kappa_x$

The role of direct interactions for $x$ and $z$ fluctuations can be explored by tuning the mean separation via the trap stiffness. A stronger trap in the $x$ direction narrows the interaction volume [see $p(R)$ in Fig. 3(b)] and increases the probability to find particles at smaller separations $R$. Figure 3(c) shows the normalized cross-correlation functions $C_x(\tau, \kappa_x)$ and $C_z(\tau, \kappa_x)$ for two distinct $\kappa_x$. For longitudinal displacements, we find two effects. First, the positive correlation strength increases in stiffer optical potentials since, for smaller separations, the influence of $\kappa_s$ increases and the motion of one particle can be transferred more directly to the other one [see Eq. (3)]. Second, the decay times $\tau_{cx} = \gamma_c/\kappa_x$ and $\tau_{rx} = \gamma_r/(2\kappa_{xs} + \kappa_x)$ decrease for increasing $\kappa_x$, since correlation effects are limited by the decay time of the trap. For $C_z$, the augmentation of direct contacts and tilting events lead to stronger negative correlations on shorter time scales. The suitability of Eq. (3) is also demonstrated in Fig. 3(d), where we choose a representative pair of trap stiffnesses $\kappa_{x1}$ and $\kappa_{x2}$ to show its effect on the cross-correlation curves $C_x$ and $C_z$.

### C. Variation of the surface potential

The interaction dynamics of the two particles depend on the reaction volume defined by $\kappa_x$ and also on the surface potential defined by $\kappa_s$. Hence, we varied the concentration of ions in the solvent and hereby the influence of electrostatic forces. It turns out that the lateral cross-correlations are a fairly sensitive measure to changes in the salt concentration $c_{\mathrm{NaCl}}$ and thereby to changes in surface charges and in Coulomb screening lengths $\Lambda \sim 1/c_{\mathrm{NaCl}}$. We find that the cross-correlations $C_z(\tau, c_{\mathrm{NaCl}})$ become more negative with increasing $c_{\mathrm{NaCl}}$ [see Fig. 4(a)]. The effect of a decreased $\Lambda$ results in a shorter mean longitudinal separation along $x$ and might enable stronger axial displacements $z_1(t)$ and $z_2(t)$ within the confining potential [see Fig. 4(b)]. Therefore, anticorrelated particle fluctuations $\langle z_1, z_2\rangle$ become more pronounced with increasing

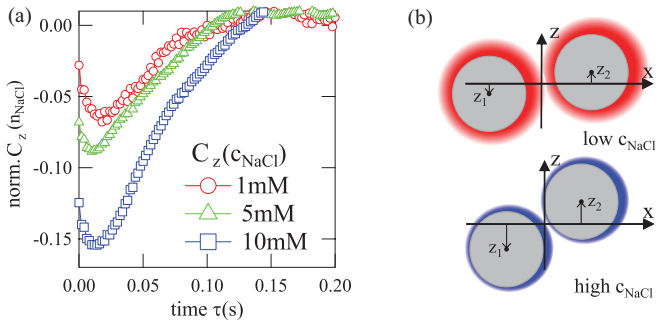


FIG. 4. (Color online) Dependence of interaction dynamics on salt concentrations. (a) Cross-correlation function for fluctuations in the $z$ direction for three different salt concentrations. (b) Longer screening lengths (low $c_{\mathrm{NaCl}}$) result in longer mean particle separations and thereby might hinder the tilting of the spheres relative to each other.

$c_{\mathrm{NaCl}}$ [Figs. 4(a) and 4(b)]. Remarkably, relative modes of motion as those distinct in the $z$ direction reveal small changes in short-range interactions more effectively than position histograms or potentials (see also S3 and Fig. S4 in Ref. [14]).

## VI. CONTACT PROBABILITY

### A. Time-differential association constant

Our tracking system enables insights into interaction processes occurring at broad temporal bandwidths. Many interactions, e.g., binding between ligand A and receptor B with concentrations $[A]$ and $[B]$ in the unbound state and $[AB]$ in the bound state, cannot be completely described by equilibrium dissociation ($k_D$) or association ($k_A$) constants, where $k_D = k_A^{-1} = ([A][B])/[AB] = \tau_{\mathrm{on}}/\tau_{\mathrm{off}} = p_{\mathrm{on}}/p_{\mathrm{off}}$. Here the probability of finding the particle in the on or off state is described by $p_{\mathrm{on,off}}$. $\tau_{\mathrm{on,off}}$ is the period the particle in in the off or on state, respectively. Often $\tau_{\mathrm{on}}$ is the time required for two binding partners to accomplish their chemical bond. Since the interaction dynamics between $A$ and $B$ are controlled by thermal fluctuations, the time-variant contact period $\tau_{\mathrm{on}}$ where the two particles are in close contact and can bind is an important parameter, which can be extracted with our tracking system at 100-$\mu$s resolution [see Fig. 5(c)]. If $n_{\mathrm{on}}(\tau_{\mathrm{on}})$ is the number of events per second to find $A$ and $B$ in close contact, $k_A \approx \frac{1}{T_{\mathrm{mes}} f_{\mathrm{scan}}} \int_{\tau_{\mathrm{min}}}^{T_{\mathrm{mes}}} n_{\mathrm{on}}(\tau_{\mathrm{on}}) d\tau_{\mathrm{on}}$ can be expressed as the average over the total measurement time $T_{\mathrm{mes}} = \sum(\tau_{\mathrm{on}} + \tau_{\mathrm{off}})$. In other words, $n_{\mathrm{on}}(\tau_{\mathrm{on}})$ acts as a time-differential association constant, allowing us to estimate the contact probability within a specific time window or reaction volume.

### B. Contact period

The two 1-$\mu$m silica beads trapped in a single optical potential serve as a model system to explore the impact of various controls. Of particular interest is the dependence of the conctact period $\tau_{\mathrm{on}}$ and the event rate $n_{\mathrm{on}}(\tau_{\mathrm{on}})$ on the effective reaction volume $\sigma_{xr}\sigma_{yr}\sigma_{zr}$. We assume that the particles are capable to react as soon as their distance falls below a certain threshold $R_0$ [Fig. 5(a)]. State transitions over a molecular potential well during $\tau_{\mathrm{on}}$, which are typically

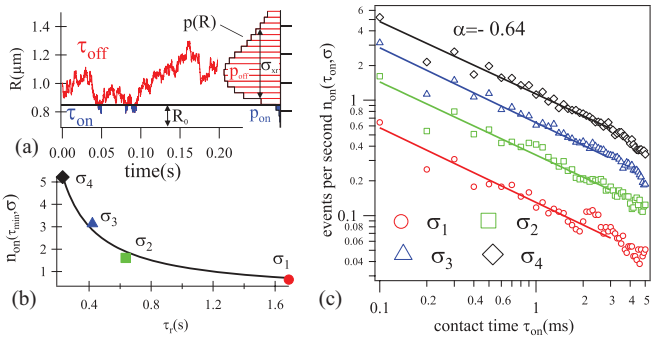


FIG. 5. (Color online) Dependence of interaction dynamics on reaction volume. (a) Relative distance trajectory $R(t)$ and position histogram $p(R)$. (b) Number of contacts for contact durations $\tau_{\min}$ as a function of the relative relaxation time. (c) Number of contacts $n_{\rm on}(\tau_{\rm on})$ as a function of contact time and various reaction volumes $\sigma$.

described by the Kramers theory, are not considered here. By controlling the effective reaction volume inside the optical trap, we are able to steer the effective particle density without introducing additional friction from nearby particles or confining walls and can study its effect on the distribution of contact periods $n_{\rm on}(\tau_{\rm on})$. The distribution of contact periods $n_{\rm on}(\tau_{\rm on})$ in Fig. 5(c) reveals that short contact times occur more frequently than longer ones.

### C. Reaction volume and relaxation time

The effective reaction volume $\sigma_{xr}\sigma_{yr}\sigma_{zr} \sim 1/\sqrt{\kappa_x\kappa_y\kappa_z}$ was varied by changing the longitudinal trap stiffness $\kappa_x$, which strongly effects the contact probability. The effective stiffness $\kappa_{xr} = (\kappa_x + 2\kappa_{xs})$ describes the width of the probability distribution $p(R,\kappa_{xr})$ of the relative bead distances $R$. Relaxation of the relative mode within the potential $V(R) = -k_BT\ln[p(R)] + V_{0r}$ occurs with the relaxation time $\tau_r = \gamma_r/(\kappa_x + 2\kappa_{xs})$ according to Eq. (3), meaning that all relative motions within $V(R)$ are governed with $\tau_r$. For short times $\tau$, where $\tau \sim 1/\gamma_r$, the distribution of contact periods shows a power-law behavior ($\alpha \approx -2/3$ for $R_0 = 0.85$ $\mu$m, $a$ = const.) which is unitary for all measured reaction volumes,

$$n_{\rm on}(\tau,\sigma_x) = a\frac{k_BT}{\gamma_r\sigma_x^2}\tau^\alpha = \frac{a}{\tau_r}\tau^\alpha. \quad (4)$$

For the shortest measurable contact period $n_{\min}$, Fig. 5(b) reveals that the contact probability $n_{\rm on}(\tau_{\min})$ is inverse proportional to the relaxation time $\tau_r$ of the relative modes and thereby nonlinearly increasing with decreasing reaction volume $\sim\sigma_{xr}$. This means, in other words, that a faster relaxation $\sim 1/\tau_r$ of the relative particle motions increases the particle interaction probability. Since the total number of contacts scales linearly with measurement time $T_{\rm mes}$ and $n_{\rm on} \sim 1/\sigma_x^2$, decreasing the interaction volume is always more effective than increasing the measurement time to enhance the reaction probability.

## VII. CONCLUSION

In conclusion, we measured fluctuation data of two beads trapped in a single potential and showed that the concept of position cross-correlations can be maintained by incorporating a short-range interaction force in the Langevin model. Differing from hydrodynamic coupling of two particles in two traps, the interplay between relative and collective modes of motion varied strongly with the direction of observation and with the delay time, which we were able measure on a very broad range from 100 $\mu$s to 2 s. Lateral position correlations turned out to be a robust and sensitive tool to resolve small changes in the interaction force as, e.g., due to different salt concentrations. Furthermore, we showed that shorter relaxation times of the relative particle motions increase their interaction probability and contact duration. The latter can be displayed as a time-differential association constant decreasing with the contact time (see S5 in Ref. [14] for details). We think that our work will be useful in colloidal sciences but also in understanding and controlling pharmaceutical or biophysical interaction processes.

## ACKNOWLEDGMENTS

We thank C. Fleck, F. Rao, D. Ruh, and L. Friedrich for fruitful discussions and a thorough reading of the manuscript. This work was supported by the DFG Grant No. RO 3615/1.

[1] D. Leckband and J. Israelachvili, Q. Rev. Biophys. **34**, 105 (2001).
[2] M. Brunner, J. Dobnikar, H.-H. von Grünberg, and C. Bechinger, Phys. Rev. Lett. **92**, 078301 (2004).
[3] J. C. Crocker and D. G. Grier, Phys. Rev. Lett. **73**, 352 (1994).
[4] J. Dhont, *An Introduction to Dynamics of Colloids* (Elsevier, Amsterdam, 1996).
[5] S. Gueron and K. Levit-Gurevich, Proc. Natl. Acad. Sci. USA **96**, 12240 (1999).
[6] D. Ruh, B. Tränkle, and A. Rohrbach, Opt. Express **19**, 1832 (2011).
[7] R. Di Leonardo, E. Cammarota, G. Bolognesi, H. Schäfer, and M. Steinhart, Phys. Rev. Lett. **107**, 044501 (2011).
[8] J.-C. Meiners and S. R. Quake, Phys. Rev. Lett. **82**, 2211 (1999).
[9] S. Henderson, S. Mitchell, and P. Bartlett, Phys. Rev. E **64**, 061403 (2001).
[10] A. Ziehl, J. Bammert, L. Holzer, C. Wagner, and W. Zimmermann, Phys. Rev. Lett. **103**, 230602 (2009).
[11] S. Martin, M. Reichert, H. Stark, and T. Gisler, Phys. Rev. Lett. **97**, 248301 (2006).
[12] M. Speidel, L. Friedrich, and A. Rohrbach, Opt. Express **17**, 7 (2009).
[13] L. Friedrich and A. Rohrbach, Opt. Lett. **35**, 1920 (2010).
[14] See Supplemental Material at http://link.aps.org/supplemental/10.1103/PhysRevE.86.021401 for movies and further details.
[15] G. Batchelor, J. Fluid Mech. **74**, 1 (1976).
[16] M. Reichert and H. Stark, Phys. Rev. E **69**, 021714 (2004).
[17] D. J. Jeffrey, Mathematika **29**, 58 (1982).
[18] L. Durlofsky, J. F. Brady, and G. Bossis, J. Fluid Mech. **180**, 21 (1987).